Supporting Information

Synthesis and Use of a Hyper-Connecting Cross-linking Agent in the Hole-transporting Layer of Perovskite Solar Cells

Brian L. Watson[1, *], Nicholas Rolston[2, *], Kevin A. Bush, Leila Taleghani, Reinhold H. Dauskardt[1,†]

[1]Department of Materials Science and Engineering, Stanford University, Stanford, CA, USA

[2]Department of Applied Physics, Stanford University, Stanford, CA, USA

Contents

S1 Characterization of Compounds

S1.1 NMR Spectra

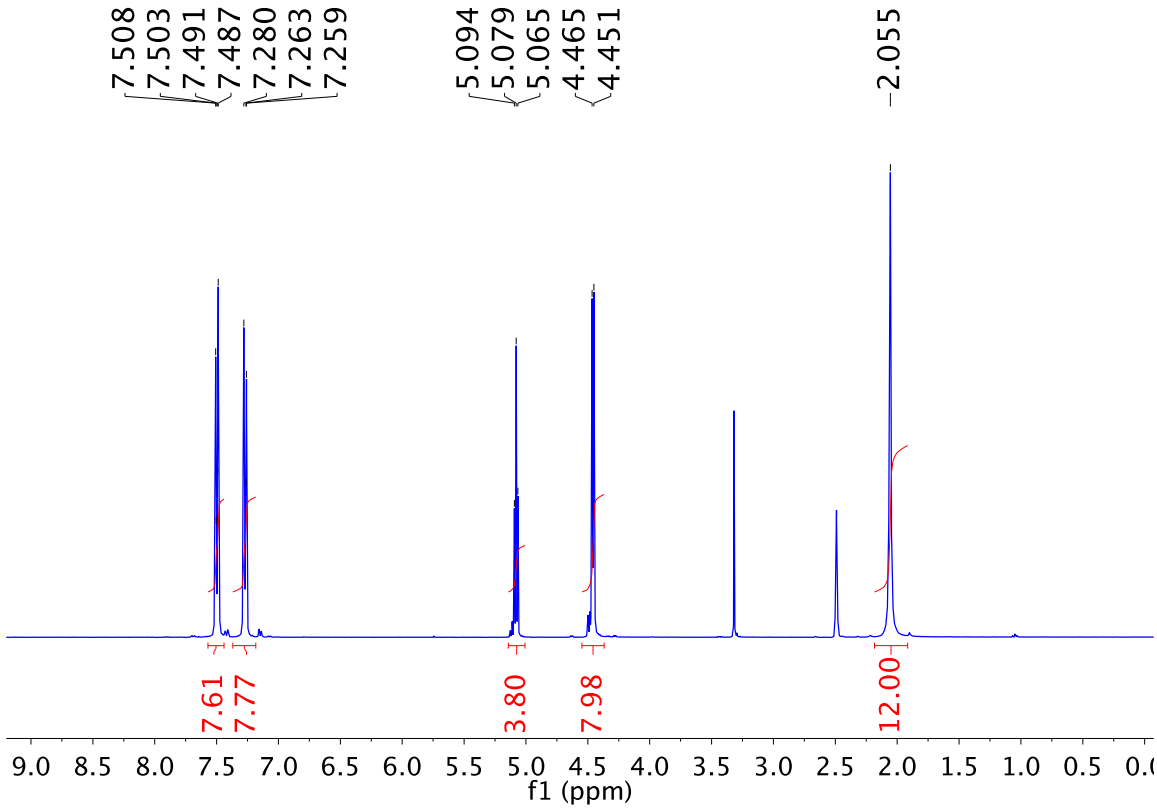

Fig. S1. ^{1}H NMR spectrum of 1,3,5,7-tetrakis-(*p*-phenylmethanol)-adamantane in DMSO-d_6

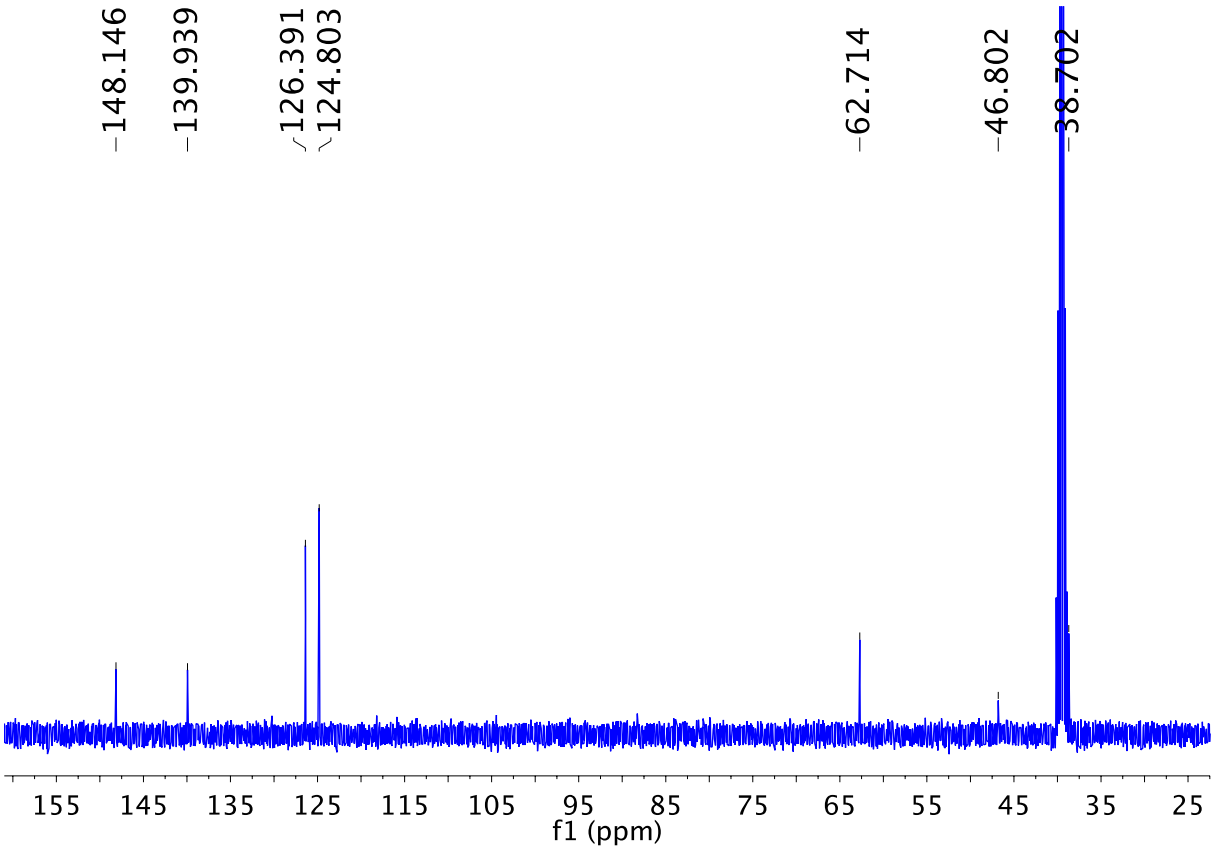

Fig. S2. ^{13}C NMR spectrum of 1,3,5,7-tetrakis-(*p*-phenylmethanol)-adamantane in DMSO-d_6.

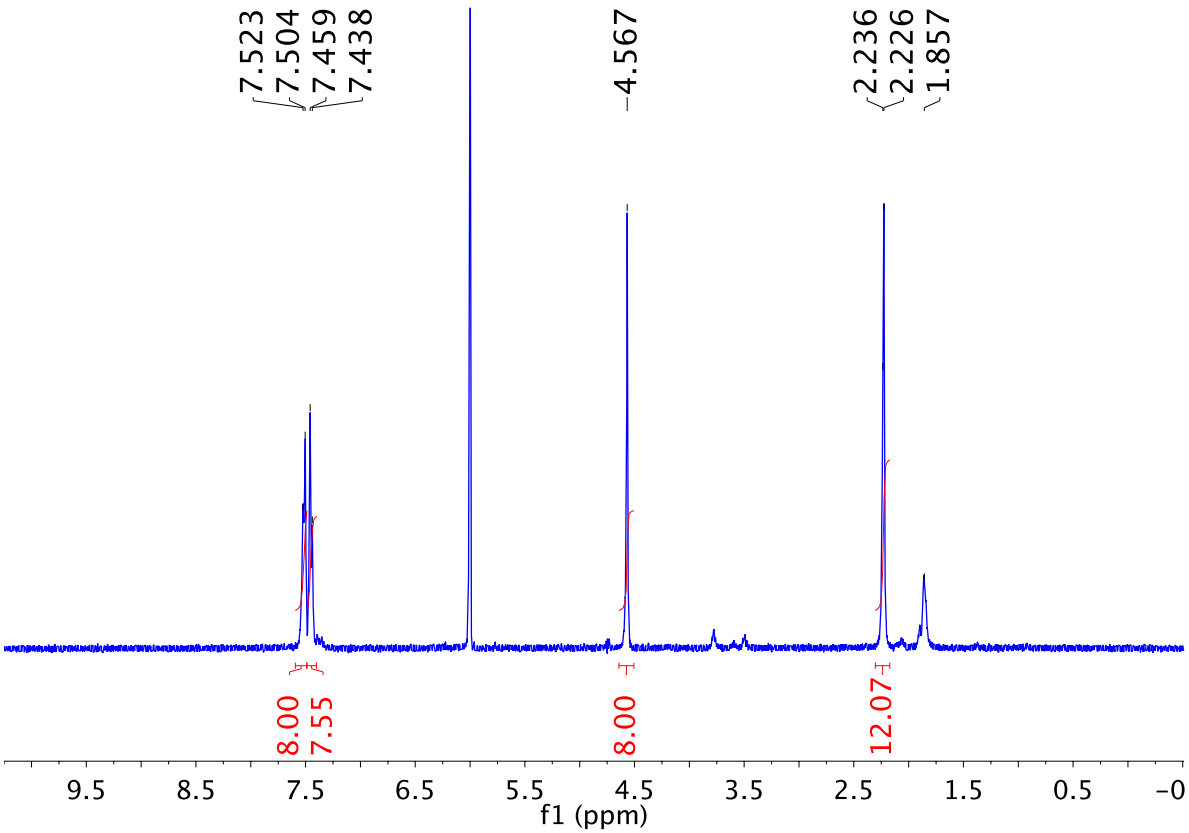

Fig. S3. ^{1}H NMR spectrum of 1,3,5,7-tetrakis-(*p*-benzylbromide)-adamantane in 1,1,2,2-tetrachlorethane-d_2 at 145 ^{o}C. Solvent peak is at 6 ppm and signal for the residual undissolved aggregate at 1.857 ppm. At RT, this peak is the dominant signal.

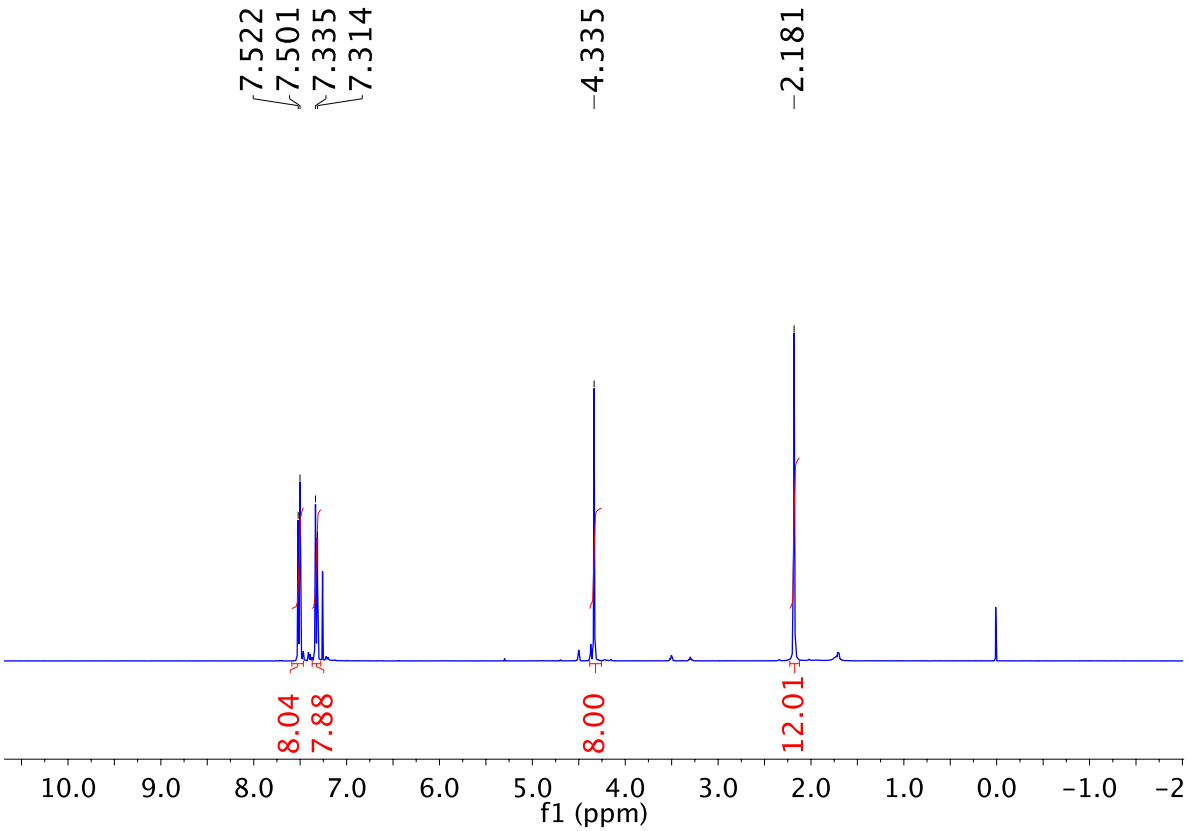

Fig. S4. ^{1}H NMR spectrum of 1,3,5,7-tetrakis-(*p*-benzylazide)-adamantane (TPBA) in $CDCl_3$.

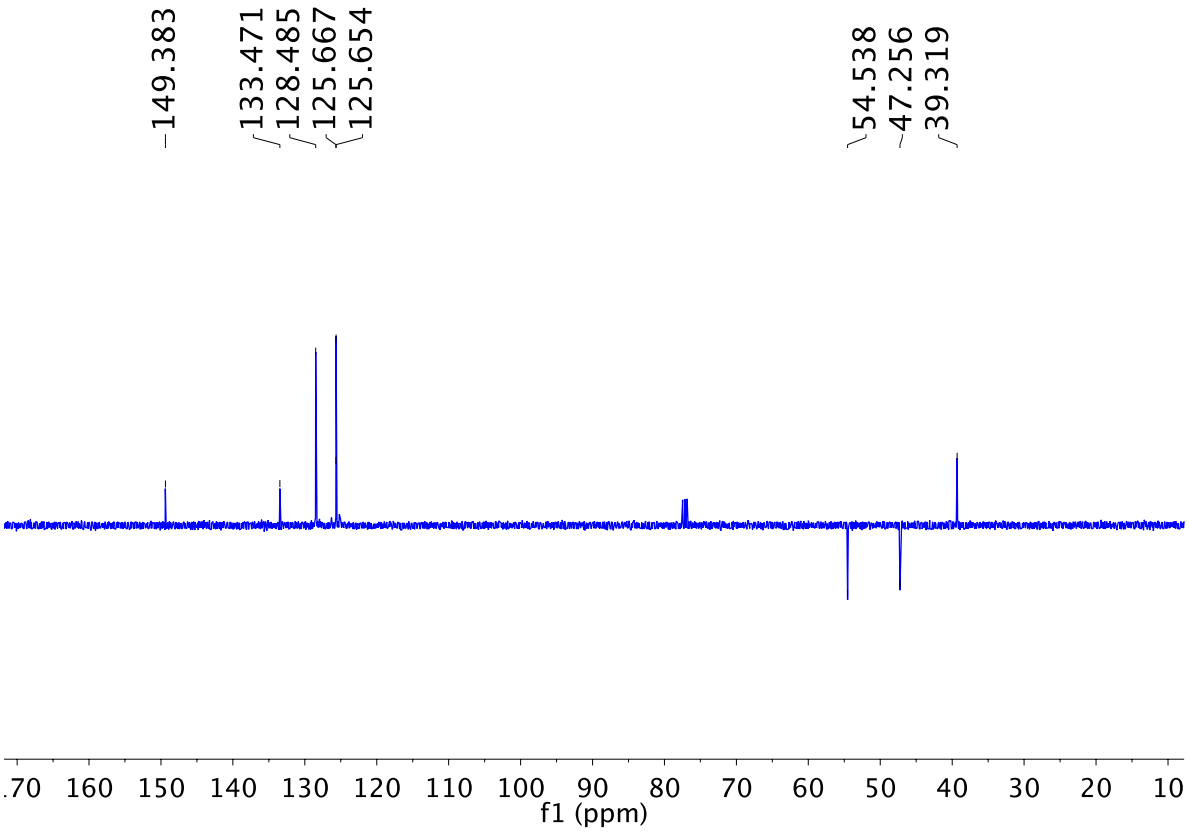

Fig. S5. DEPT ^{13}C NMR spectrum of 1,3,5,7-tetrakis-(*p*-benzylazide)-adamantane (TPBA) in $CDCl_3$.

S1.2 ATR Spectra

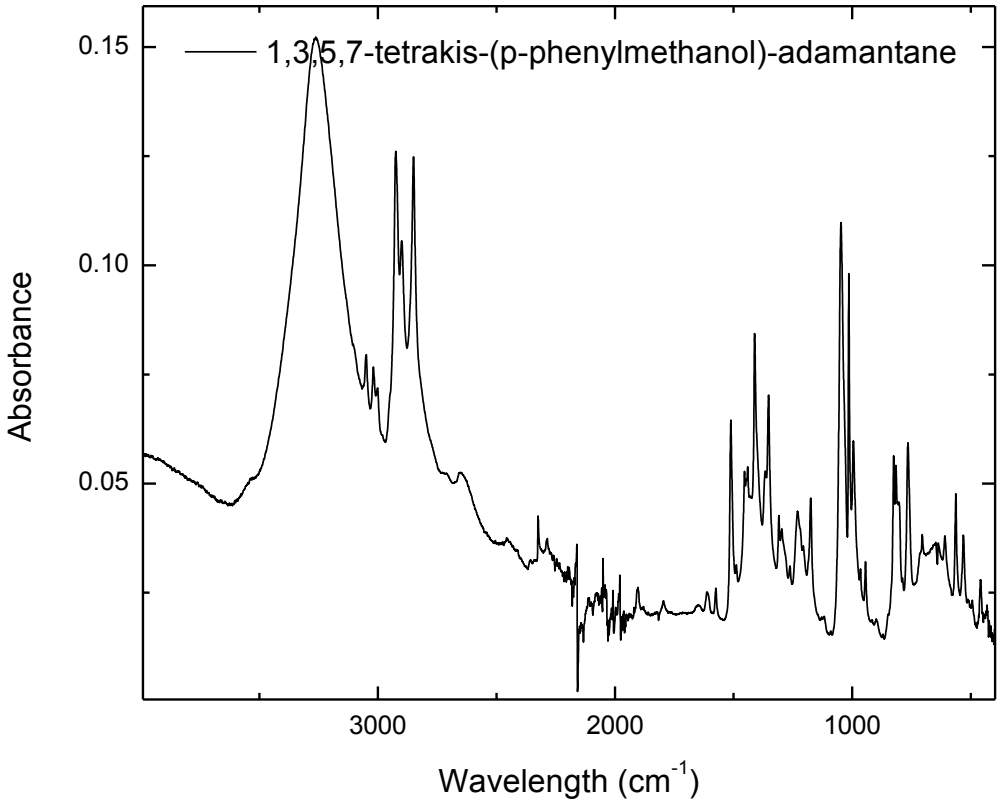

Fig. S6. ATR spectrum of 1,3,5,7-tetrakis-(p-phenylmethanol)-adamantane.

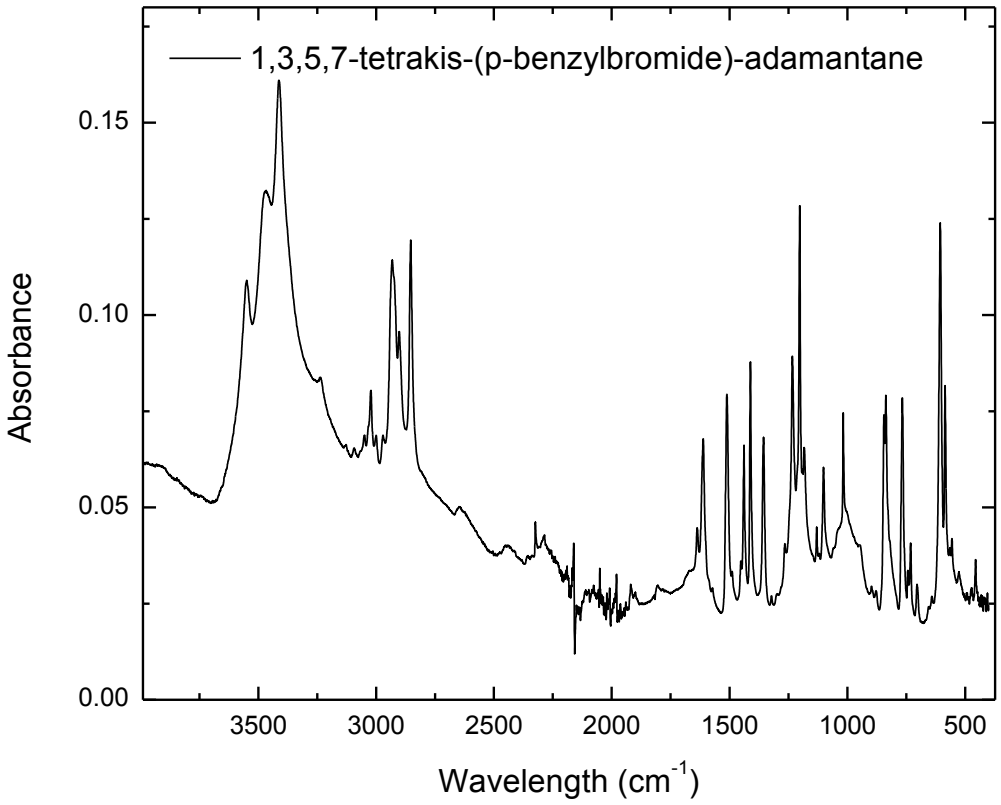

Fig. S7. ATR spectrum of 1,3,5,7-tetrakis-(p-benzylbromide)-adamantane.

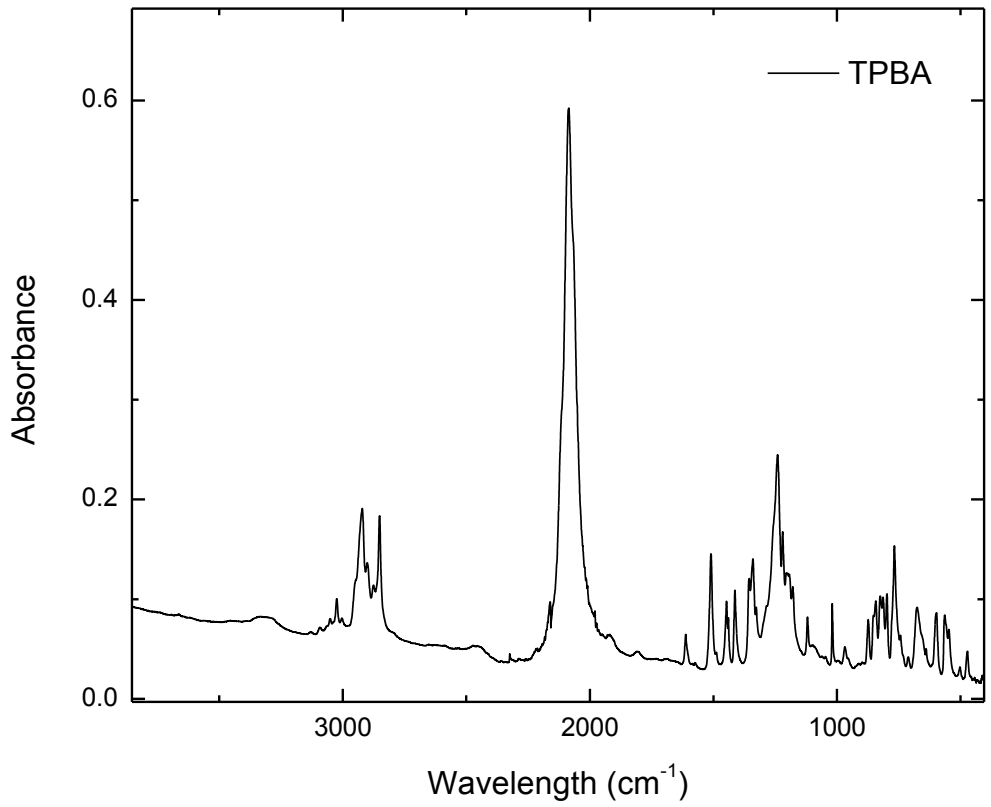

Fig. S8. ATR spectrum of TPBA

S2.4 HR Mass Spectra

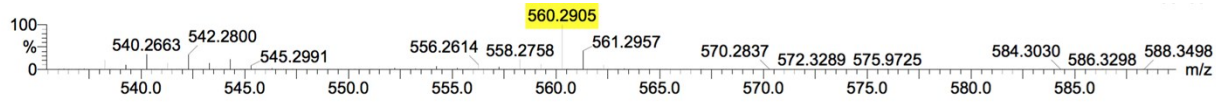

Minimum:				-1.5		
Maximum:		3.0	10.0	200.0		
Mass	Calc. Mass	mDa	PPM	DBE	i-FIT	Formula
560.2905	560.2900	0.5	0.9	20.0	13.8	C34 H36 N6 O2
	560.2913	-0.8	-1.4	19.5	4.1	C36 H38 N3 O3
	560.2918	-1.3	-2.3	7.0	908.1	C22 H40 N8 O9
	560.2886	1.9	3.4	20.5	52.9	C32 H34 N9 O
	560.2886	1.9	3.4	15.0	42.5	C33 H40 N2 O6
	560.2927	-2.2	-3.9	19.0	23.0	C38 H40 O4
	560.2932	-2.7	-4.8	6.5	707.8	C24 H42 N5 O10
	560.2873	3.2	5.7	15.5	105.3	C31 H38 N5 O5
	560.2940	-3.5	-6.2	24.0	81.6	C39 H36 N4
	560.2945	-4.0	-7.1	11.5	512.3	C25 H38 N9 O6
	560.2860	4.5	8.0	16.0	198.6	C29 H36 N8 O4
	560.2860	4.5	8.0	10.5	205.0	C30 H42 N O9
	560.2953	-4.8	-8.6	23.5	148.9	C41 H38 N O
	560.2958	-5.3	-9.5	11.0	367.5	C27 H40 N6 O7

Fig. S9. EI Mass spectrum report of 1,3,5,7-tetrakis-(*p*-phenylmethanol)-adamantane: $C_{38}H_{40}O_4$.

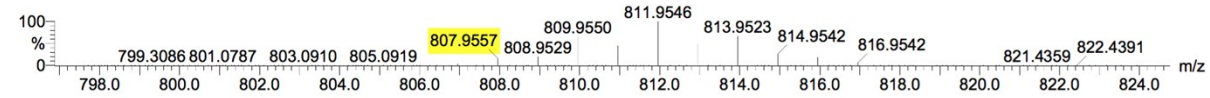

Minimum:				-1.5		
Maximum:		3.0	10.0	200.0		
Mass	Calc. Mass	mDa	PPM	DBE	i-FIT	Formula
807.9557	807.9558	-0.1	-0.1	26.5	2661.2	C37 H25 N5 O2 Br3
	807.9556	0.1	0.1	6.5	3917.5	C24 H38 N5 O6 Br4
	807.9556	0.1	0.1	49.0	9942.7	C48 H5 N6 O4 Br
	807.9553	0.4	0.5	29.0	4631.0	C35 H18 N6 O8 Br2
	807.9561	-0.4	-0.5	4.0	4320.8	C26 H45 N4 Br5
	807.9563	-0.6	-0.7	14.0	3904.0	C23 H27 N10 O8 Br3
	807.9550	0.7	0.9	19.0	2807.8	C38 H36 Br4
	807.9548	0.9	1.1	-1.0	4508.8	C25 H49 O4 Br5
	807.9566	-0.9	-1.1	28.5	4506.6	C37 H20 N3 O9 Br2

Fig. S10. EI Mass spectrum report of 1,3,5,7-tetrakis-(*p*-bromobenzyl)-adamantane: $C_{38}H_{36}Br_4$.

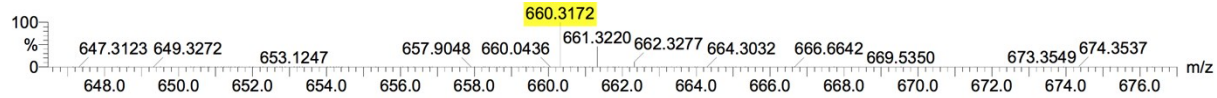

Minimum:				-1.5		
Maximum:		3.0	10.0	200.0		
Mass	Calc. Mass	mDa	PPM	DBE	i-FIT	Formula
660.3172	660.3173	-0.1	-0.2	22.0	3.5	C37 H40 N8 O4
	660.3173	-0.1	-0.2	16.5	14.5	C38 H46 N O9
	660.3178	-0.6	-0.9	15.0	1103.9	C22 H36 N20 O5
	660.3178	-0.6	-0.9	9.5	1130.5	C23 H42 N13 O10
	660.3164	0.8	1.2	10.0	1392.6	C21 H40 N16 O9
	660.3159	1.3	2.0	22.5	30.9	C35 H38 N11 O3
	660.3159	1.3	2.0	17.0	37.4	C36 H44 N4 O8
	660.3186	-1.4	-2.1	21.5	5.5	C39 H42 N5 O5
	660.3186	-1.4	-2.1	27.0	12.7	C38 H36 N12
	660.3191	-1.9	-2.9	14.5	867.7	C24 H38 N17 O6
	660.3151	2.1	3.2	10.5	1685.7	C19 H38 N19 O8

Fig. S11. EI Mass spectrum report of 1,3,5,7-tetrakis-(*p*-benzylazide)-adamantane: $C_{38}H_{36}Br_4$.

S2 UV-Vis spectra of TPBA and PTAA-X films

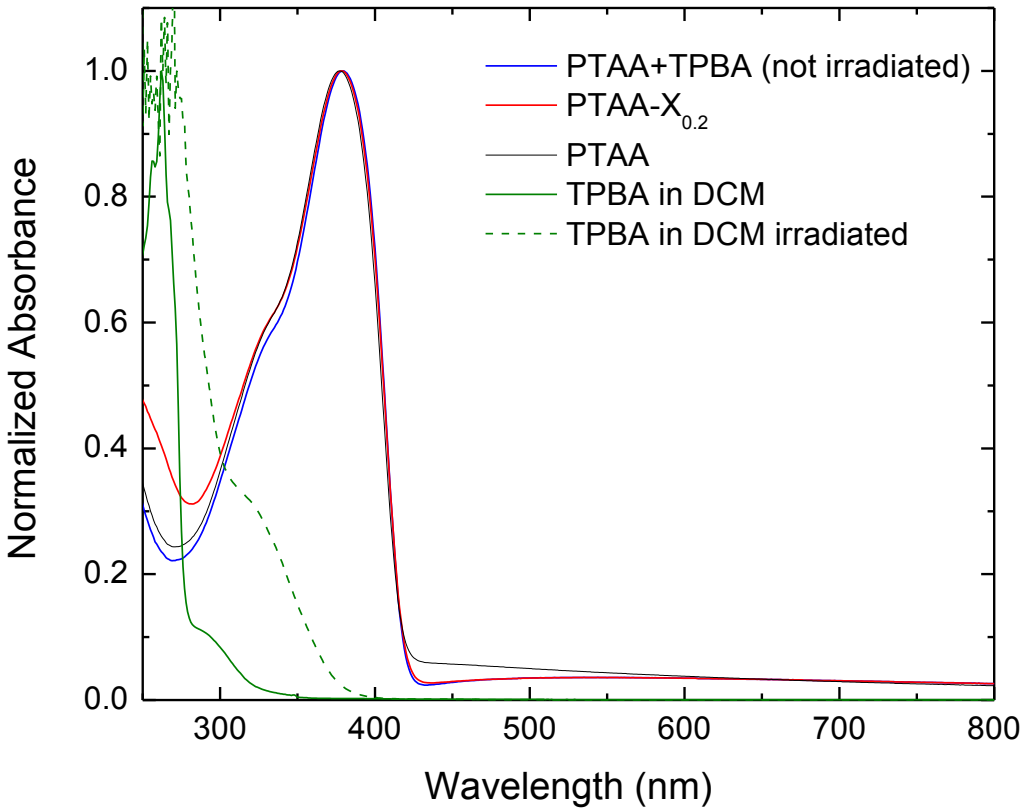

Fig. S12. UV-Vis spectrum of TPBA in dichloromethane without (green) and with UV-C irradiation (green dashed) and of PTAA, PTAA with 0.2 w.eq. of TPBA, and PTAA-$X_{0.2}$ in which the TPBA has been UV-C irradiate to induce cross-linking.

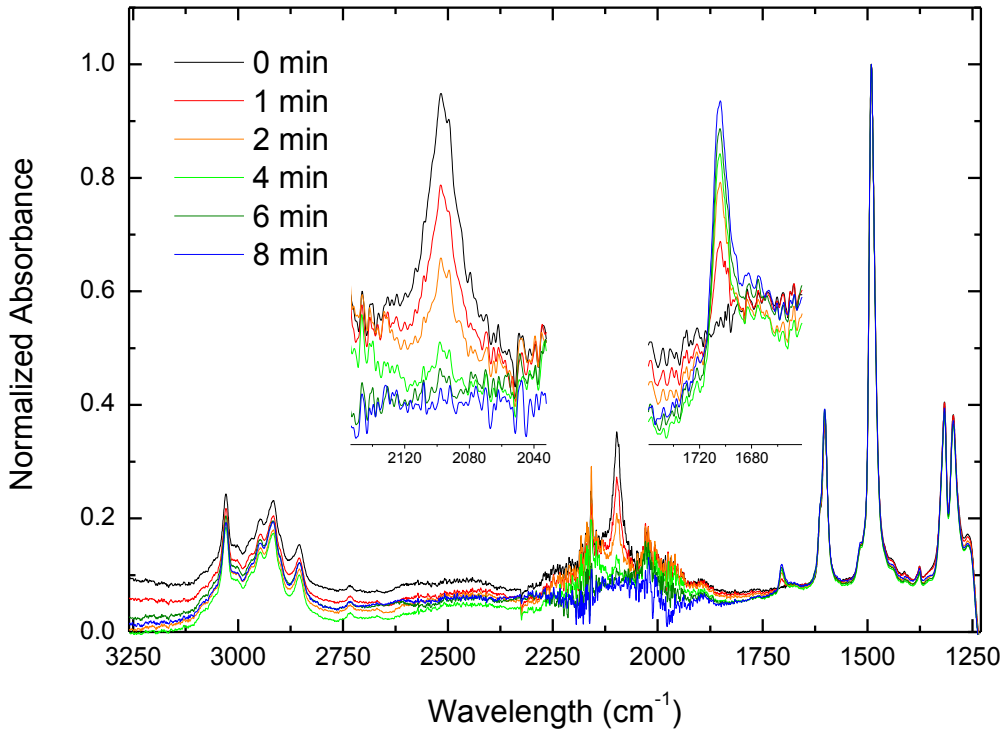

Fig. S13. Evolution of the ATR spectra of PTAA films containing 0.2 w.e.q. TPBA with UV-C irradiation. The strong absorbance at 2082 cm^{-1} of the azide group of TPBA decreases with UV-C dosage while a new weakly absorbing peak growing in at 1710 cm^{-1}.

S3 Solvent Resistance

Films were deposited on freshly cleaned silicon beams from solutions prepared as described above with the following compositions: PTAA-$X_{0.01}$, PTAA-$X_{0.05}$, PTAA-$X_{0.1}$ and PTAA-$X_{0.2}$. Following UV-C irradiation, films were dipped for 30 seconds in toluene, removed and allowed to air dry. Films were inspected visually for etching of the deposited film.

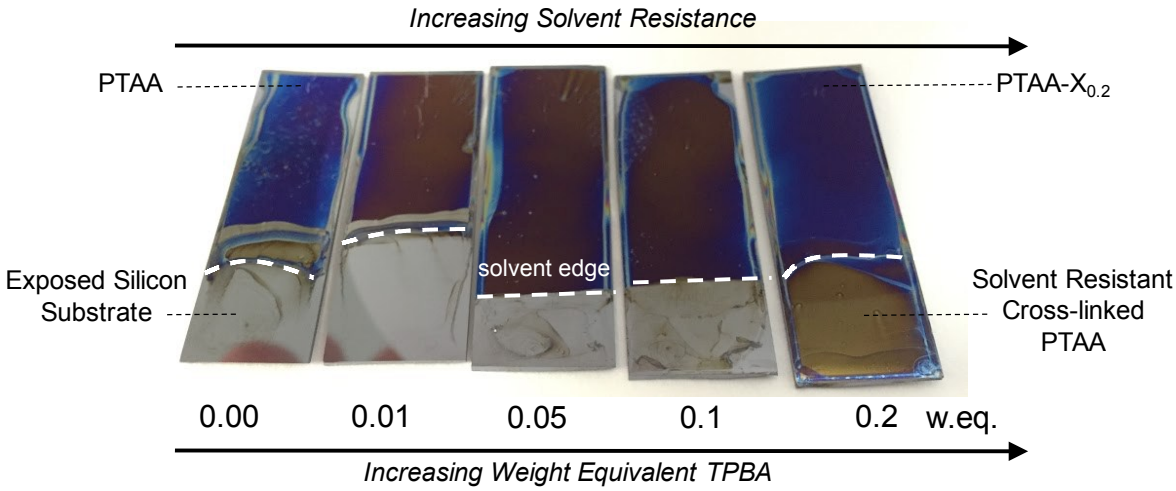

Fig. S14. Films of PTAA with increasing concentrations of TPBA deposited on silicon and irradiated with UV-C for cross-linking were dipped in toluene for 30 s, and dried. Resistance to dissolution is achieved by addition of 0.2 w.eq of TPBA. For lower concentrations, the solvent exposure readily dissolves the PTAA film exposing the silicon substrate below the dashed white lines indicating the solvent edge.

S4 XPS Spectra

After mechanical testing, a survey x-ray photoelectron spectroscopy (XPS, PHI 5000 Versaprobe) scan (0 - 1000 *eV*) was made of each of the fractured specimens using monochromatic Al K_α x-ray radiation at 1487 *eV* to locate the fracture path and thus the weakest layer or interface within the test structure.

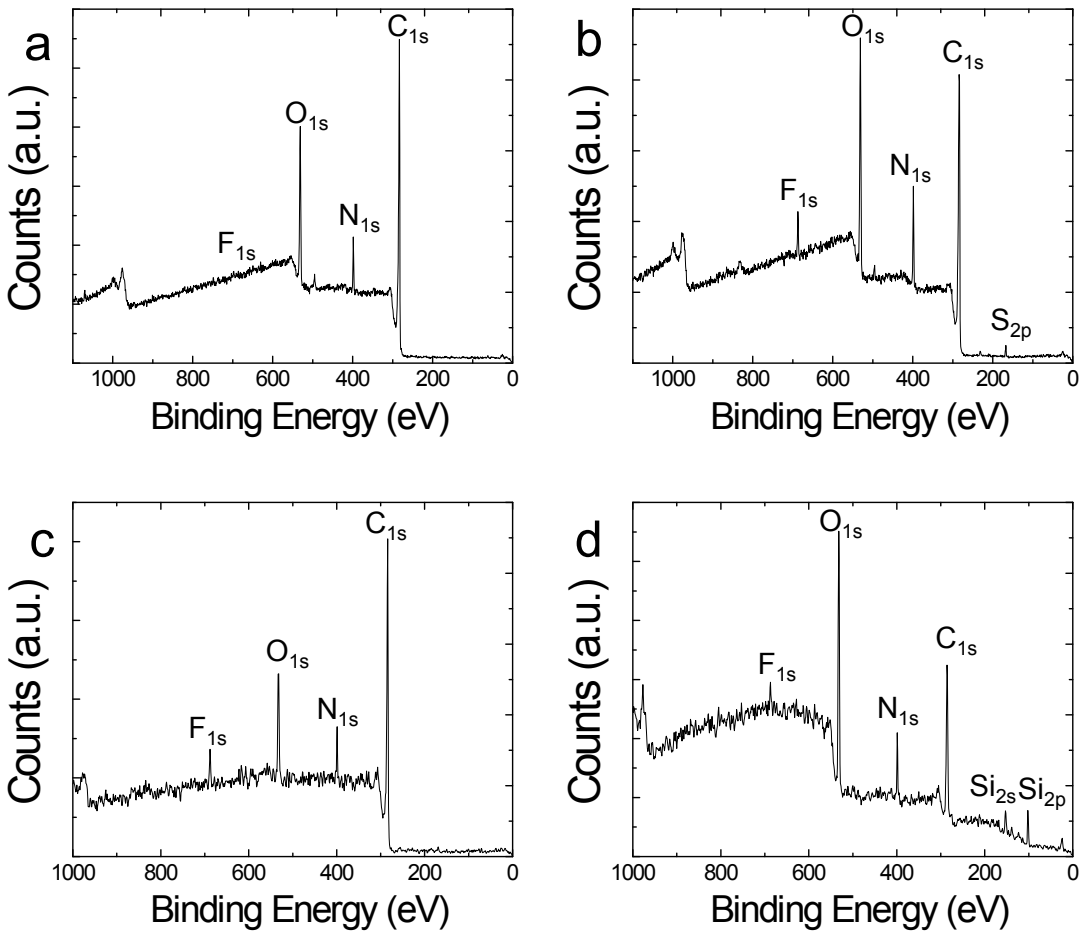

Fig. S15. XPS spectra of the fractured halves of the a) Al side and b) glass side of AzPTMS-treated glass with d-PTAA, showing cohesive failure and of the c) Al side and d) glass side of untreated glass with d-PTAA, showing adhesive failure at the d-PTAA/glass interface.

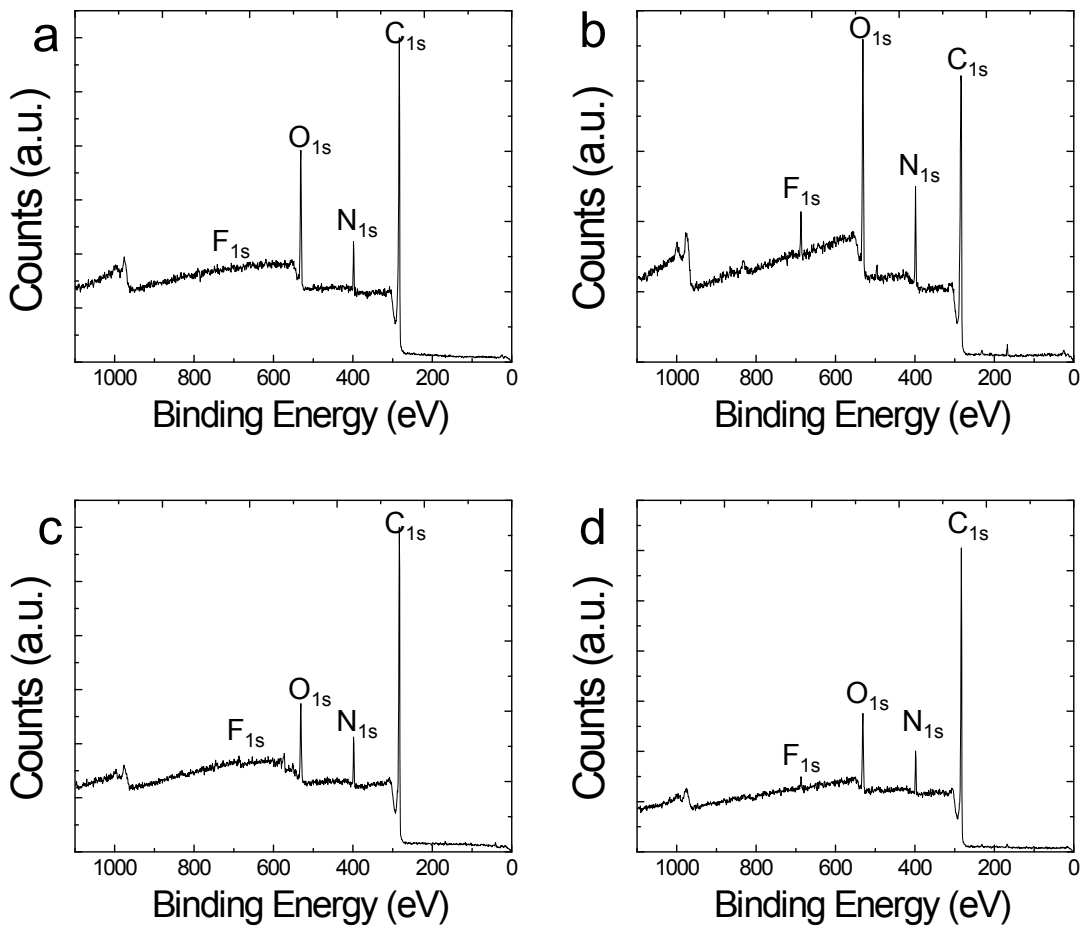

Fig. S16. XPS spectra of the fractured halves of the a) Al side and b) glass side of AzPTMS-treated glass with PTAA, showing cohesive failure and of the c) Al side and d) glass side of AzPTMS-treated glass with PTAA-X, showing cohesive failure.

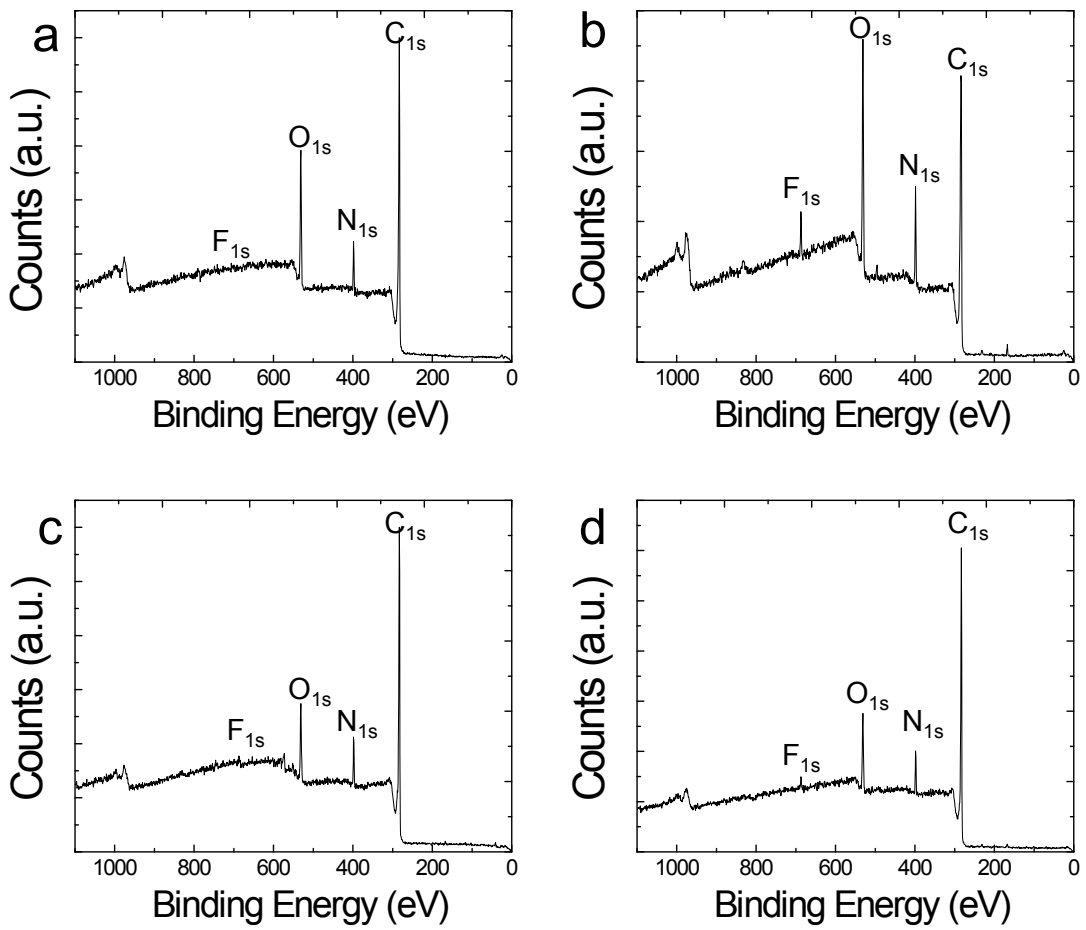

Fig. S17. XPS spectra of the fractured halves of the a) Al side and b) glass side of AzPTMS-treated glass with doped-PTAA, showing cohesive failure and of the c) Al side and d) glass side of AzPTMS-treated glass with doped-PTAA-X, showing cohesive failure.

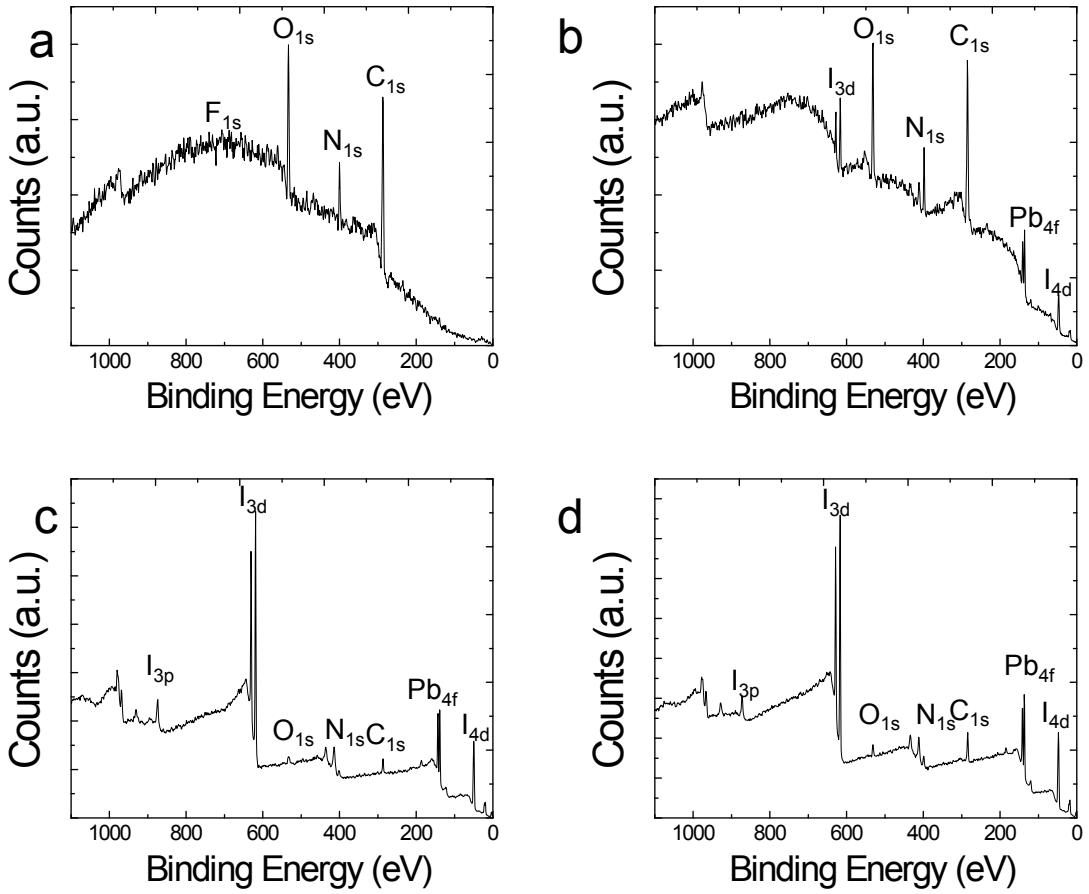

Fig. S18. XPS spectra of the fractured halves of the a) Al side and b) glass side of d-PTAA coated perovskite on glass, showing adhesive failure at the d-PTAA/perovskite interface and of the c) Al side and d) glass side of d-PTAA-X coated perovskite on glass, showing cohesive failure.

S5 Max Power Point Tracking

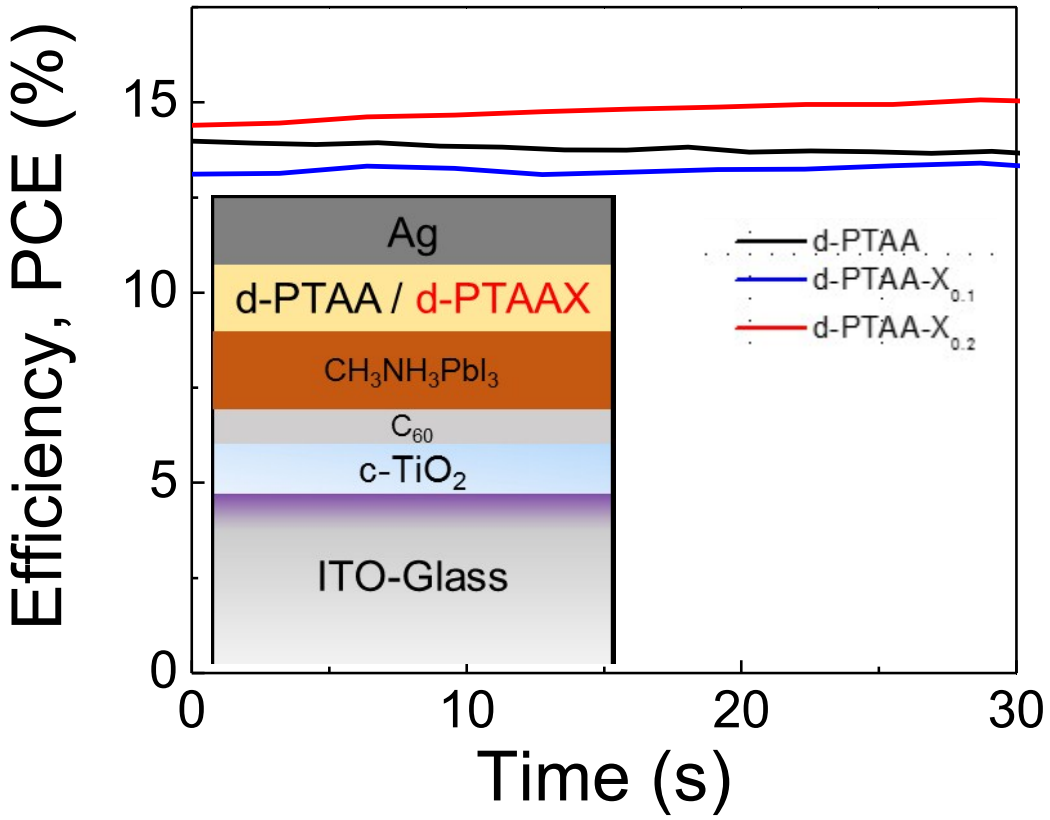

Fig. S19. Maximum power point tracking of efficiency of representative conventional (n-i-p) perovskite solar cells with varying amounts of TBPA.

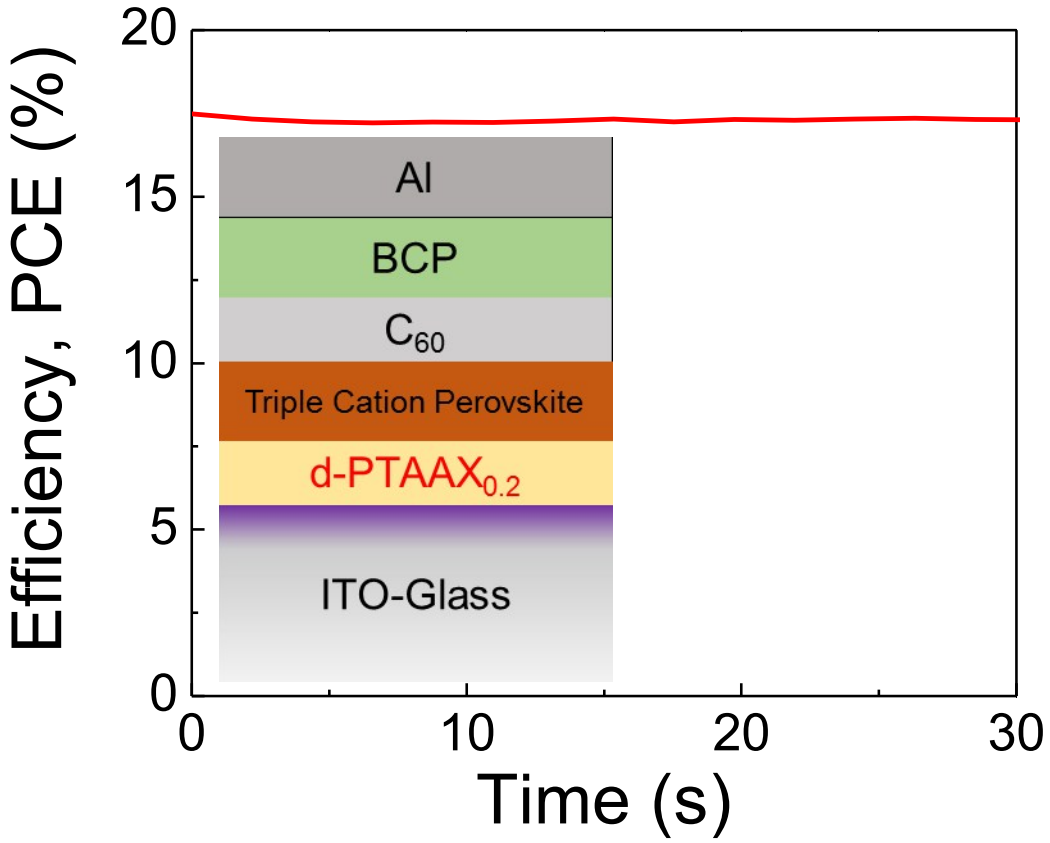

Fig. **S20.** Maximum power point tracking of representative inverted (p-i-n) perovskite solar cell with TBPA.